Hindawi
Journal of Advanced Transportation
Volume 2023, Article ID 6649871, 15 pages
https://doi.org/10.1155/2023/6649871

Research Article

Mixed Integer Linear Programming Based Speed Profile Optimization for Heavy-Haul Trains

Huazhen Yu,[1] Yihui Wang,[1] Andrea D'Ariano,[2] Anzheng Lai,[1] and Youneng Huang [1,3]

[1]*School of Electronic and Information Engineering, Beijing Jiaotong University, Beijing 100044, China*
[2]*Department of Civil, Computer Science and Aeronautical Technologies Engineering, Roma Tre University, Rome 00146, Italy*
[3]*National Engineering Research Center of Rail Transportation Operation and Control System, Beijing Jiaotong University, Beijing 100044, China*

Correspondence should be addressed to Youneng Huang; ynhuang@bjtu.edu.cn

Received 20 April 2023; Revised 18 September 2023; Accepted 28 October 2023; Published 27 December 2023

Academic Editor: Maria Vittoria Corazza

Automatic heavy-haul train (HHT) operation technology has recently received considerable attention in the field of rail transportation. In this paper, a discrete-time-based mathematical formulation is proposed to address the speed profile optimization problem in order to ensure the safe, efficient, and economical operation of heavy-haul trains (HHTs). Due to the presence of long and steep downgrades (LSDs) on some heavy-haul lines, the brake forces of the HHT are typically jointly determined by air braking and electric braking. The time characteristics of the air braking, such as the command delay and the change process caused by the air pressure, are taken into account, and then formulas are presented to calculate the air brake force. In addition, the influence of the neutral section on the control of the electric braking is considered via space-based constraints. The resulting problem is a nonlinear optimal control problem. To achieve linearization, auxiliary 0-1 binary variables and the big-M approach are introduced to transform the nonlinear constraints regarding slope, curve, neutral section, air brake force, and air-filled time into linear constraints. Moreover, piecewise affine (PWA) functions are used to approximate the basic resistance of the HHT. Finally, a mixed integer linear programming (MILP) model is developed, which can be solved by CPLEX. The experiments are carried out using data from a heavy-haul railway line in China, and the results show that the proposed approach is effective and flexible.

1. Introduction

Heavy-haul transportation is of great importance for improving transport efficiency, increasing economic profits, and lowering transport costs. It has developed rapidly in many countries. Specifically, the axle load of heavy-haul trains (HHTs) has increased significantly to improve the transport capacity, which in turn presents higher requirements for the drivers of HHTs. Moreover, the increase in weight and size of HHTs is also limited by the infrastructure and the hauling capacity of the locomotives. In particular, the application of the automatic train operation (ATO) system for HHTs [1–3] has attracted increasing attention from researchers in recent years, compared with the traditional manual operation.

With the increasing demand for iron ore year by year in Australia, the AutoHaul system [2] developed by Rio Tinto has been applied to achieve autonomous heavy-haul train (HHT) operation in 2018. There are three main benefits to this endeavour in preference to manual operation. The first is to increase productivity by shortening cycle times and eliminating stops for driver changes. Furthermore, operating costs would be reduced with fewer drivers and lower fuel consumption. The third is to reduce the possibility of driver error, thereby improving the safety of HHT operations. However, the implementation of the ATO system in Chinese HHTs is a challenging open issue due to the differences in HHT speed control methods between Australia and China. Specifically, HHTs in Australian railways have achieved automatic operation through the electronically controlled

pneumatic (ECP) braking mode, which allows all wagons to receive control commands consistently [4]. HHTs in China are still equipped with conventional air brake systems, where control commands are delivered with a transmission delay depending on the speed of the air wave and the length of the HHT.

Although there has been much research on the application of ATO in Chinese urban rail transit [5–7]. Researchers have mainly focused on the following two critical issues: the speed profile optimization that can be achieved off-line and the train speed controller design with real-time performance. In order to achieve improved performance of train operation, there are still many challenges in the operation of HHTs. Passenger trains, such as urban rail trains and high-speed trains, are mainly controlled by traction and electric braking, which has higher control accuracy and faster response time than air braking; in particular, air braking is only applied when the electric brake force is too small to stop the train at low speed without considering the effect on the next regime. For HHTs, due to their large tractive mass and many sections with long and steep downgrades (LSDs), air braking and electric braking should be applied collaboratively to keep the speed within the given limits, i.e., speed limit and minimum release speed. In particular, we note that the air braking should be applied intermittently for the operation of HHTs on LSDs, as shown in Figure 1. This strategy is also known as the cyclic air braking, where the driver should consider when to apply or release the air brakes and the amount of pressure reduction, taking into account the effect on the next brake application or release, until the trains have left the LSDs [8]. In addition, electric braking prevents the sharp increase in the speed of HHTs and makes the air-filled times of the train pipes more sufficient. It is noted that the electric brake force should be equal to zero when HHTs are running in a neutral section.

Train speed profile optimization [9, 10] is commonly formulated as an optimal control problem aimed at enhancing train operation performance by optimizing the outputs like regime sequences and switching points. This study centers on the optimization of strategies aimed at ensuring the safe, efficient, and economical operation of HHTs on LSDs. While various approaches like pontryagin maximum principle (PMP) [11], approximate dynamic programming (ADP) [12, 13], quadratic programming (QP) [14, 15], mixed integer linear programming (MILP) [16], and heuristic algorithms (HAs) [17–19] have been used to develop HHT operation strategies, there exists a notable gap in the discussions pertaining to critical aspects. Specifically, the time characteristics of air braking, and a constraint within engineering applications where power supply is interrupted while travelling through the neutral section, have not been adequately addressed. Furthermore, the cycle air braking strategy was not taken into consideration in [14, 15], warranting further investigation. In addition, the complexity of line conditions makes it challenging for the PMP to yield optimal solutions, while the results obtained from both ADP and HAs are approximate solutions. On the other hand, mathematical programming methods like QP and MILP benefit

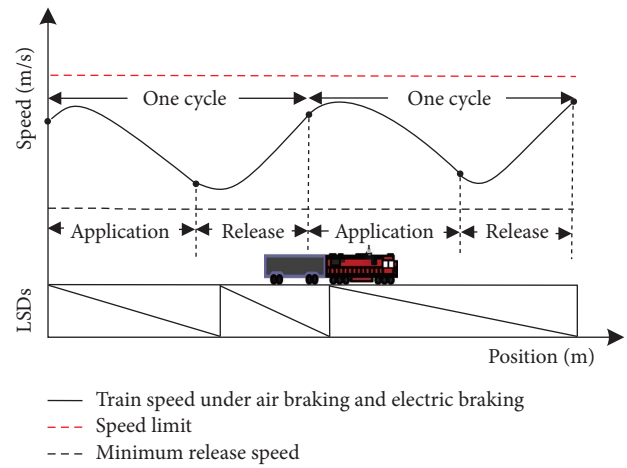

Figure 1: Diagram of the HHT operation on LSDs.

from mature commercial solvers that ensure the identification of globally optimal solutions [20, 21]. This study was conducted building upon the aforementioned discussion. The main contributions of this paper are summarized as follows:

(1) A formula is developed to calculate air brake force, considering time characteristics for the first time. Subsequently, a discrete-time-based MILP model is presented to optimize the HHT speed profile. In this model, the total running time is divided into multiple intervals.

(2) Real-world line conditions and operational constraints, including slopes, neutral sections, and air-filled times, are considered. To facilitate approximate linearization, the big-M approach and binary variables are introduced.

(3) A hybrid scheme that integrates coarse-grained and fine-grained models is devised to strike a balance between computation efficiency and accuracy. Then this complex challenge is tackled by using the well-known solver CPLEX. Moreover, a series of experiments are conducted to demonstrate the solutions achieved.

The remainder of this paper is organized as follows. Section 2 delves into the existing literature concerning the optimization of HHT operation strategies. Section 3 outlines the model of the HHT running on LSDs integrating a neutral section. Moving forward, the discrete-time-based MILP approach is given in Section 4. The effectiveness and flexibility of the proposed approach are validated through simulation experiments in Section 5. Finally, conclusions are drawn in Section 6.

2. Literature Review

The optimization of train operation has been aptly described as an optimal control problem, as noted in [5]. Various optimization methods have been employed to improve the operation performance of long HHTs.

In early years, the researchers from the Scheduling and Control Group (SCG) of the University of South Australia developed the FreightMiser system to reduce fuel consumption for long-haul trains, and optimal speed profiles for relatively simple scenarios, such as isolated steep uphill or downhill sections, were obtained using PMP [22]. Subsequently, another PMP-based approach was proposed in [11] for the purpose of energy saving, which considered the operation requirements of a Chinese HHT. However, the pursuit of rigorous mathematical solutions led to model simplification, ignoring factors such as changing slopes and air braking characteristics. With the improvement of computing power, recent years have witnessed a multistage decision process to determine the control sequence for HHTs running on LSDs, where lookup-table-based [12] and value-iteration-based [13] ADP were used to yield safety-centric, cost-effective, and operationally efficient driving strategies. The advent of deep Q-network (DQN) [23] mitigated the challenge of high-dimensional spaces by approximating action-value functions with neural networks. Furthermore, a QP-based approach was developed to address the multiobjective trajectory optimization problem in the context of HHTs. This approach encompassed considerations of key constraints, including line resistance, neutral section, as well as traction and electric braking, as highlighted in [14]. Moreover, a purposeful selection scheme was designed to obtain the optimal weighting factors [15]. Notably, these investigations were conducted on railway scenarios characterized by less intricate line conditions and the absence of LSDs. In addition, HAs find predominant application in resolving the HHT operation strategy on LSDs due to their less stringent model requirements. For instance, to ensure safety and improve efficiency during operations, methods like particle swarm optimization (PSO) [17], genetic algorithm (GA) [18], and artificial bee colony (ABC) [19] have been embraced. These algorithms enable the identification of optimized switching points for air brake application and release. In the realm of optimizing train speed profiles, MILP has established itself as a widely recognized and effective method. Its utility spans across urban rail trains [24–26], high-speed trains [27, 28], and medium-speed maglev trains [29]. Notably, it has recently been employed in the domain of HHT [16], where the linearization description of the air brake force and the air-filled time constraint is not well treated and still full of challenges.

However, in the aforementioned studies, when addressing air braking, the force was calculated using empirical formulas on the assumption of instantaneous characteristics due to the complex working principle of the air brake system, and the delay of air brake application or release, as well as the progression of air brake force alteration were overlooked. Moreover, real constraints such as the neutral section were not given due consideration. To highlight achievements and gaps in existing research, a brief comparison of the most relevant literature is presented in Table 1.

3. Model Formulation

3.1. Assumptions. In this paper, we make the following assumptions:

(1) The pressure reduction for brake control typically ranges from 50 to 140 kPa in intervals of 10 kPa. On lines with LSDs, a pressure reduction of 50 kPa can be employed to control the speed of the HHT. It is important to note that routine stops and stops resulting from suboptimal control are not taken into account.

(2) The output for electric brake control is expressed as a ratio of the characteristic curve.

3.2. Notations. For a better understanding of the paper, Table 2 lists the notations used in this section.

3.3. Longitudinal Dynamics of the HHT. In this paper, the HHT is regarded as a rigid multimass model when running on the line, as in [30], to reduce unnecessary complexity.

When the HHT with n cars runs on LSDs, $n = n_l + n_w$, n_l is the number of locomotives and n_w is the number of wagons. $M_t = \sum_{i=1}^{n} m_i$, i is the index of cars and m_i is the mass of car i. The continuous-time model of the HHT moving along the track is expressed as follows:

$$M_t \frac{\mathrm{d}v}{\mathrm{d}t} = -F_e(v) - F_a(v,t) - F_b(v) - F_l(s), \tag{1a}$$

$$\frac{\mathrm{d}s}{\mathrm{d}t} = v, \tag{1b}$$

where s is the position of the HHT, M_t and v are the mass and speed of the HHT, t is the time of the HHT running, F_e is the electric brake force provided by the locomotives, F_a is the air brake force acting on all cars, and F_b and F_l are the basic and line resistances.

3.3.1. Resistance. The basic resistance [31], related to the speed of the train, can be expressed as follows:

$$F_b = \sum_{i=1}^{n} m_i f_{b,t} g \times 10^{-3}, \tag{2}$$

where $f_{b,t} = a_1 + b_1 v + c_1 v^2$ [32], a_1, b_1, and c_1 are positive coefficients related to the type of car. g denotes the gravity constant. As the number of locomotives is much smaller than that of wagons, it can be assumed that the unit basic resistance of a locomotive is the same as that of a wagon.

The line resistances [31] composed by the slope and curve resistances can be computed as follows:

$$F_l = \left(\sum_{i=1}^{n} m_i I_i + \sum_{i=1}^{n} m_i \frac{D}{C_i} \right) g \times 10^{-3}, \tag{3}$$

where D is the empirical coefficient.

For the position of the car i, the gradient is measured by I_i‰ and the curve resistance can be calculated by the curve radius C_i, which can be described by the following piecewise linear functions:

Table 1: Comparison of relevant publications on method and model.

Publication	Method	Objective	Considering neutral section	Time characteristics of air brake force	LSDs
Lin et al. [11]	PMP	SA, EC	Not	Not	Yes
Wang et al. [12]	ADP	SA, MC	Not	Not	Yes
Su et al. [13]	ADP	SA, MC, OE	Not	Not	Yes
Bai et al. [14]	QP	SA, EC, PU, SM	Yes	Not	Not
Li et al. [15]	QP	SA, EC, PU, SM	Not	Not	Not
Su et al. [16]	MILP	SA, MC, OE	Not	Yes	Yes
Yu et al. [17]	PSO	SA, OE	Not	Not	Yes
Yu et al. [18]	GA	SA, OE	Not	Not	Yes
Huang et al. [19]	ABC	SA, EC, MC, OE	Yes	Not	Yes
Benjamin et al. [22]	PMP	SA, EC	Not	Not	Not
Liu et al. [23]	DQN	SA, MC, OE	Not	Not	Yes
This study	MILP	SA, MC, OE	Yes	Yes	Yes

SA: safety, EC: energy consumption, MC: maintenance cost, OE: operation efficiency, PU: punctuality, SM: smoothness.

$$I_i(x_i) = \begin{cases} I'_1, s_0 \le x_i \le s_1, \\ I'_2, s_1 \le x_i \le s_2, \\ \cdots \\ I'_{n_g}, s_{n_g-1} \le x_i \le s_{n_g}, \end{cases} \tag{4a}$$

$$C_i(x_i) = \begin{cases} C'_1, s'_0 \le x_i \le s'_1, \\ C'_2, s'_1 \le x_i \le s'_2, \\ \cdots \\ C'_{n_c}, s'_{n_c-1} \le x_i \le s'_{n_c}, \end{cases} \tag{4b}$$

where x_i is the position of car i, $l_{i-1,i}$ is the physical length between cars $i-1$ and i, and $x_1 = s, x_i = s - l_{i-1,i}, i = 2, 3, \cdots, n$; $s_0, s_1, \cdots, s_{n_g-1}, s_{n_g}$ are the starting and ending positions of slopes, $I'_1, I'_2, \cdots, I'_{n_g}$ are the gradient of slopes; $s'_0, s'_1, \cdots, s'_{n_c-1}, s'_{n_c}$ are the starting and ending positions of curves, and $C'_1, C'_2, \cdots, C'_{n_c}$ are the radius of curves.

3.3.2. Electric Brake Force. The electric brake force [31] can be formulated as follows:

$$F_e = u_e F_{e,\max}(v), \tag{5}$$

where u_e is the output ratio and $F_{e,\max}$ is the maximum electric brake force that can be achieved according to the characteristics of a locomotive.

3.3.3. Air Brake Force. The air brake force [31] is generated by compressed air, and it can be calculated as follows:

$$F_a = \sum_n n_s K_i \cdot \varphi_i, \tag{6}$$

where for car i, K_i is the pressure acting on each brake shoe, and φ_i is the brake shoe friction coefficient. n_s is the number of brake shoes equipped on a car.

$$K_i = \frac{\pi}{4n_s} d_b^2 P_i^a n_b \eta_b \gamma_b \cdot 10^{-6}, \tag{7a}$$

$$\varphi_i = 0.41 \cdot \frac{K_i + 200}{4K_i + 200} \cdot \frac{3.6v + 150}{2 \times 3.6v + 150}, \tag{7b}$$

where d_b is the diameter of the brake cylinder, η_b is the transmission efficiency of the braking device, γ_b is the braking leverage, and n_b is the number of brake cylinders equipped on a car.

In equation (7a), $C = \pi d_b^2 n_b \eta_b \gamma_b \cdot 10^{-6}/4n_s$ is a constant for a given brake system. Therefore, the description of the brake cylinder pressure P_i^a is the key to calculating the air brake force. Based on the function proposed in [33] and test data, the mathematical formulations are as follows:

$$P_i^a = u_b P_{b,i}(t, \Delta p) + u_r P_{r,i}(t, \Delta p), \tag{8a}$$

$$P_{b,i}(t, \Delta p) = \begin{cases} 0, t_a^b \le t < t_a^b + t_{b,i}, \\ f_a^b, t_a^b + t_{b,i} \le t < t_a^b + t_{b,i} + t_{\max}^b, \\ P_{a,\max}, t \ge t_a^b + t_{b,i} + t_{\max}^b, \end{cases} \tag{8b}$$

$$P_{r,i}(t, \Delta p) = \begin{cases} P_{a,\max}, t_a^r \le t < t_a^r + t_{r,i}, \\ f_a^r, t_a^r + t_{r,i} \le t < t_a^r + t_{r,i} + t_{\min}^r, \\ 0, t \ge t_a^r + t_{r,i} + t_{\min}^r, \end{cases} \tag{8c}$$

where $P_{b,i}$ and $P_{r,i}$ are the pressure of the brake cylinder of car i during air brake application and release, u_b and u_r are the binary variables indicating the application and release of the air brake, Δp denotes the amount of pressure reduction, t_a^b and t_a^r are the timing of the air brake application and release, and $t_{b,i}$ and $t_{r,i}$ are the delay times for car i at which the pressure begins to rise and fall, depending on the propagation speed of the wave. $t_{\max}^b$ and $t_{\min}^r$ are the times required for the pressure to change to the maximum value $P_{a,\max}$ and zero, and f_a^b and f_a^r are the functions that describe the processes of air brake application (pressure rise) and air brake release (pressure fall) for each car.

Table 2: Notations for model formulation.

Notation	Description
i	Index of cars
m_i	Mass of car i
n_l, n_w	Number of locomotives and wagons
M_t	Mass of the HHT
v	Speed of the HHT
s	Position of the HHT
t	Time of HHT running
F_b, F_l	Basic and line resistances
F_a	Air brake force
F_e	Electric brake force
$f_{b,t}$	Unit basic resistance
a_1, b_1, c_1	Positive coefficients of basic resistance
g	Gravity constant
x_i	Position of car i
I_i	Gradient at the position of car i
n_g	Number of slopes
$I'_1, \cdots, I'_{n_g}$	Gradient of slopes
$s_0, \cdots, s_{n_g}$	Starting and ending positions of slopes
C_i	Curve radius at the position of car i
n_c	Number of curves
$C'_1, \cdots, C'_{n_c}$	Radius of curves
$s'_0, \cdots, s'_{n_c}$	Starting and ending positions of curves
D	Empirical coefficient
$l_{i-1,i}$	Length between cars $i-1$ and i
u_e	Output ratio of electric brake force
$F_{e,\max}$	Maximum electric brake force
n_s	Number of brake shoes equipped on a car
K_i	Pressure acting on one brake shoe of car i
φ_i	Brake shoe friction coefficient of car i
d_b	Brake cylinder diameter
γ_b	Braking leverage
n_b	Number of brake cylinders equipped on a car
η_b	Transmission efficiency of braking device
P_i^a	Brake cylinder pressure of car i
$P_{b,i}$	Brake cylinder pressure of car i during air brake application
$P_{r,i}$	Brake cylinder pressure of car i during air brake release
Δp	Amount of pressure reduction
u_b, u_r	Binary variable indicating regimes of the application and release of air braking

Table 2: Continued.

Notation	Description
t_a^b, t_a^r	Timing of air brake application and release
$t_{b,i}$, $t_{r,i}$	Pressure rise and fall delay times for car i
$t_{\min}^r$	Time required for the pressure to change to zero
$t_{\max}^b$	Time required for the pressure to change to the maximum value
$P_{a,\max}$	Maximum value of brake cylinder pressure
f_a^b, f_a^r	Functions to describe the rise and fall of brake cylinder pressure for each car
T	Given running time
T_b	Application time of air braking
$S_{\max}$	Running distance with the speed limit
S	Total running distance
w_1, w_2	Weight coefficients
$v_{\lim}$	Speed limit
v_r	Minimum release speed
t_r	Air brake release time
t_f	Air-filled time
s_b, s_e	Starting and ending positions of a neutral section

3.4. Optimization Problem

3.4.1. Objective. Given a specific running time, the pursuit of enhanced operation efficiency necessitates a higher average speed, thereby maximizing the covered distance. Besides, to mitigate the wear of brake shoes caused by elevated temperatures and reduce maintenance cost, the duration of air brake application must be minimized.

The running distance S and the air brake application time T_b can be calculated by

$$S = \int_0^T v \, \mathrm{d}t, \tag{9a}$$

$$T_b = \int_0^T u_b \, \mathrm{d}t. \tag{9b}$$

The objective function can be written as follows:

$$\min O\,\mathrm{bj} = w_1 \frac{T_b}{T} - w_2 \frac{S}{S_{\max}}, \tag{10}$$

where w_1 and w_2 are weight coefficients, $w_1 + w_2 = 1$. $S_{\max}$ is the running distance when the HHT runs at maximum speed (see below "speed limit"). T is the given running time of the HHT.

3.4.2. Constraints. Train dynamic constraint: The movement of the HHT should follow equations (1a) and (1b).

Speed constraints: For safety, trains cannot run above the speed limit $v_{\lim}$ or below the minimum release speed v_r. When the speed is lower than v_r, the in-train force will increase and the coupler may even break.

$$v_r \le v \le v_{\lim}. \tag{11}$$

Electric brake constraint: Generally, $0 \le F_e \le F_{e,\max}$, that is, the output of the electric brake force should not be greater than the maximum electric brake force. So in this paper, the following set should be satisfied.

$$0 \le u_e \le 1. \tag{12}$$

Air brake constraints: "$u_b = 1$" denotes application and "$u_r = 1$" denotes release, the relationship between them can be described as follows:

$$u_b + u_r = 1, u_b \in \{0, 1\}, u_r \in \{0, 1\}. \tag{13}$$

The rated pressure of the brake pipe is set at 500 or 600 kPa, with a chosen output of 50 kPa when the HHT is navigating on lines with LSDs.

$$\Delta p = 50\,\mathrm{kPa}. \tag{14}$$

Besides, to allow sufficient time for the train pipe to be filled, a release interval between adjacent air brake applications must be at least as long as the air-filled time.

$$t_r \ge t_f, \tag{15}$$

where t_r is the air brake release time, and t_f is the air-filled time.

Neutral section constraint: For the neutral section of the electric railway, the output of the electric brake force equates to zero, which can be rewritten as follows:

$$F_e = 0, \quad s_b \le s \le s_e, \tag{16}$$

where s_b and s_e are the starting position and ending position of a neutral section, respectively.

4. Solution Approach

The given running time is divided into N intervals. $T = \sum_{k=1}^{N} \Delta t$, and in each interval $[t_k, t_{k+1}]$, values of the speed limit, the slope resistance, and the curve resistance are constant; we also assume that the traction or braking force is taken as constant. Note that $t_1 = t_{\text{start}} = 0$ and $t_N = t_{\text{end}} = T$, t_{start} and t_{end} are the beginning and ending times.

4.1. Decision Variables. Table 3 presents the decision variables for optimizing the speed profile of the HHT.

4.2. MILP Approach. Inspired by [24], the optimization problem described in Section 3 was solved using the MILP approach. Specifically, the trajectory optimization problem of passenger trains was studied in [24], and a discrete-space-based model was obtained, with kinetic energy per unit mass $E = 0.5v^2$ and time t as state variables, and position s as the independent variable. In this paper, a discrete-time-based model has been established, with speed v and position s as state variables, and time t as the independent variable. In addition, the modelling of the air brake force and the air-filled time of the train pipe are the focus, and the neutral section, the gradient and the curve radius are all piecewise functions related to the position. Binary variables must therefore be introduced to achieve linearization.

PWA functions are used to realize the linearization, and the nonlinear function $F_b(v)$, equation (2), can be written as a piecewise linear function of $F_{b,k}$,

$$F_{b,k} = \begin{cases} \mu_{1,k} v_k + \theta_{1,k}, v_k \le v_{1,k}, \\ \mu_{2,k} v_k + \theta_{2,k}, v_k \ge v_{1,k}, \end{cases} \tag{17}$$

where the values of $\mu_{1,k}$, $\mu_{2,k}$, $\theta_{1,k}$, $\theta_{2,k}$, and $v_{1,k}$ are determined by the fitting process.

Besides, $F_e(v)$, $F_a(v,t)$, and $F_l(s)$ can be written as the form: $F_e(v) = F_{e,k}$, $F_a(v,t) = F_{a,k}$, and $F_l(s) = F_{l,k}$. So defining $\xi = -1/M_t$, $\eta_{r,k} = -\mu_{r,k}/M_t$, $\gamma_{r,k} = -\theta_{r,k}/M_t$, and $r = \{1, 2\}$, the model in equation (1a) can be rewritten as follows:

$$\frac{\mathrm{d}v}{\mathrm{d}t} = \xi\left(F_{e,k} + F_{a,k} + F_{l,k}\right) + \eta_{r,k} v_k + \gamma_{r,k}, \tag{18}$$

Table 3: Decision variables for speed profile optimization.

Notation	Description
$u_{e,k}$	Output ratio of electric brake force at k stage
$u_{b,k}$	Binary variable indicating whether air braking is applied or not at k stage, if yes, $u_{b,k} = 1$; otherwise, $u_{b,k} = 0$
$u_{r,k}$	Binary variable indicating whether air braking is released or not at k stage, if yes, $u_{r,k} = 1$; otherwise, $u_{r,k} = 0$

Then, the zero-order holder and the trapezoidal integration rule are used to obtain the discrete-time dynamic model:

$$v_{k+1} = a_{r,k}v_k + b_{r,k}\left(F_{e,k} + F_{a,k} + F_{l,k}\right) + c_{r,k}, \tag{19a}$$

$$s_{k+1} = s_k + \frac{1}{2}\Delta t\left(v_k + v_{k+1}\right), \tag{19b}$$

where $a_{r,k} = e^{\eta_{r,k}\Delta t}$, $b_{r,k} = (e^{\eta_{r,k}\Delta t} - 1)\xi/\eta_{r,k}$, and $c_{r,k} = (e^{\eta_{r,k}\Delta t} - 1)\gamma_{r,k}/\eta_{r,k}$; $v_1 = v_0$, $s_1 = 0$, and v_0 are the initial speeds of the HHT.

According to the properties introduced in [34], the PWA model in equation (19a) can be transformed as follows:

$$\begin{aligned} v_{k+1} = {} & \left(a_{1,k} - a_{2,k}\right)z_{1,k} + \left(b_{1,k} - b_{2,k}\right)h_{1,k} \\ & + \left(c_{1,k} - c_{2,k}\right)\delta_{1,k} + a_{2,k}v_k \\ & + b_{2,k}\left(F_{e,k} + F_{a,k} + F_{l,k}\right) + c_{2,k}. \end{aligned} \tag{20}$$

Here, the auxiliary logical variables $\delta_{1,k}$, $z_{1,k}$, and $h_{1,k}$ are defined to transform the model

$$\left[v_k \le v_{1,k}\right] \Longleftrightarrow \left[\delta_{1,k} = 1\right], \tag{21a}$$

$$z_{1,k} = \delta_{1,k}v_k, \tag{21b}$$

$$h_{1,k} = \delta_{1,k}\left(F_{e,k} + F_{a,k} + F_{l,k}\right). \tag{21c}$$

Therefore, the following linear constraints should be satisfied:

$$\begin{cases} v_k \le v_{1,k} + \left(v_{\max,k} - v_{1,k}\right)\left(1 - \delta_{1,k}\right), \\ v_k \ge v_{1,k} + \varepsilon + \left(v_{\min,k} - v_{1,k} - \varepsilon\right)\delta_{1,k}, \end{cases} \tag{22a}$$

$$\begin{cases} z_{1,k} \le \delta_{1,k}v_{\max,k}, \\ z_{1,k} \ge \delta_{1,k}v_{\min,k}, \\ z_{1,k} \ge v_k - v_{\max,k}\left(1 - \delta_{1,k}\right), \\ z_{1,k} \le v_k - v_{\min,k}\left(1 - \delta_{1,k}\right), \end{cases} \tag{22b}$$

$$\begin{cases} h_{1,k} \le \delta_{1,k}\left(F_{e,\max} + F_{a,\max} + F_{l,\max}\right), \\ h_{1,k} \ge \delta_{1,k}\left(F_{e,\min} + F_{a,\min} + F_{l,\min}\right), \\ h_{1,k} \ge \left(F_{e,k} + F_{a,k} + F_{l,k}\right) - \left(F_{e,\max} + F_{a,\max} + F_{l,\max}\right)\left(1 - \delta_{1,k}\right), \\ h_{1,k} \le \left(F_{e,k} + F_{a,k} + F_{l,k}\right) - \left(F_{e,\min} + F_{a,\min} + F_{l,\min}\right)\left(1 - \delta_{1,k}\right), \end{cases} \tag{22c}$$

where $F_{e,\min}$ and $F_{e,\max}$ are the minimum and maximum electric brake force, $F_{a,\min}$ and $F_{a,\max}$ are the minimum and maximum air brake force, $F_{l,\min}$ and $F_{l,\max}$ are the minimum and maximum line resistance, and notably, ε is a positive small number.

For equations (4a) and (4b), binary variables are introduced to describe these piecewise linear functions:

$$\begin{cases} \varsigma_{i,k}^{1} + \varsigma_{i,k}^{2} + \cdots + \varsigma_{i,k}^{n_g} = 1, \\ I_{i,k}\left(x_{i,k}\right) = \varsigma_{i,k}^{1} I_1' + \varsigma_{i,k}^{2} I_2' + \cdots + \varsigma_{i,k}^{n_g} I_{n_g}', \\ x_{i,k} \le s_1 \varsigma_{i,k}^{1} + s_2 \varsigma_{i,k}^{2} + \cdots + M_1 \varsigma_{i,k}^{n_g}, \\ x_{i,k} \ge s_1 \varsigma_{i,k}^{2} + s_2 \varsigma_{i,k}^{3} \cdots + s_{n_g-1} \varsigma_{i,k}^{n_g}, \\ \varsigma_{i,k}^{1}, \varsigma_{i,k}^{2}, \cdots, \varsigma_{i,k}^{n_g} \in \{0,1\}, \end{cases} \tag{23a}$$

$$\begin{cases} \alpha_{i,k}^{1} + \alpha_{i,k}^{2} + \cdots + \alpha_{i,k}^{n_c} = 1, \\ C_{i,k}\left(x_{i,k}\right) = \alpha_{i,k}^{1} C_1' + \alpha_{i,k}^{2} C_2' + \cdots + \alpha_{i,k}^{n_c} C_{n_c}', \\ x_{i,k} \le s_1' \alpha_{i,k}^{1} + s_2' \alpha_{i,k}^{2} + \cdots + M_1 \alpha_{i,k}^{n_c}, \\ x_{i,k} \ge s_1' \alpha_{i,k}^{2} + s_2' \alpha_{i,k}^{3} \cdots + s_{n_c-1}' \alpha_{i,k}^{n_c}, \\ \alpha_{i,k}^{1}, \alpha_{i,k}^{2}, \cdots, \alpha_{i,k}^{n_c} \in \{0,1\}, \end{cases} \tag{23b}$$

where M_1 is a positive large number, $x_{1,k} = s_k$, $x_{i,k} = s_k - l_{i-1,i}, i = 2, 3, \cdots, n$.

Based on equations (6)–(8c), the total air brake force of the HHT can be obtained and expressed as a function of time for the specific pressure reduction.

$$F_{a,k} = u_{b,k} f_b(t) + u_{r,k} f_r(t), \tag{24}$$

where f_b and f_r are the functions of air brake force and time during brake application and release, respectively. Here, when $v \in [9.72, 20.83]$m/s, the value range of $(3.6v + 150)/(2 \times 3.6v + 150)$ is from 0.75 to 0.84, which is not large. So, in equation (7b), the average speed $\overline{v}$ is used for the calculation. Then, we define $F_{a,k}^{b} = u_{b,k} f_b(t)$ and $F_{a,k}^{r} = u_{r,k} f_r(t)$; equation (24) can be rewritten as $F_{a,k} = F_{a,k}^{b} + F_{a,k}^{r}$. Next, general recursive expressions are proposed to calculate the air brake force, taking into account the time characteristics and the effects of historical regimes:

$$F_{a,k}^{b} = u_{b,k} f_0^{b} + u_{b,k-1} u_{b,k}\left(f_1^{b} - f_0^{b}\right) + \cdots + u_{b,k-n_b} u_{b,k-n_b+1} \cdots u_{b,k-1} u_{b,k}\left(f_{n_b}^{b} - f_{n_b-1}^{b}\right), \tag{25a}$$

$$F_{a,k}^{r} = u_{r,k} f_0^{r} + u_{r,k-1} u_{r,k}\left(f_1^{r} - f_0^{r}\right) + \cdots + u_{r,k-n_r} u_{r,k-n_r+1} \cdots u_{r,k-1} u_{r,k}\left(f_{n_r}^{r} - f_{n_r-1}^{r}\right), \tag{25b}$$

where n_b and n_r are number of the selected values used in force calculation for air brake application and release. $f_0^{b} = 0$, $f_1^{b} = f_b(t_a^{b} + \Delta t)$, $f_2^{b} = f_b(t_a^{b} + 2\Delta t)$, $\cdots$, $f_{n_b-1}^{b} = f_b(t_a^{b} + (n_b - 1)\Delta t)$, $f_{n_b}^{b} = F_{a,\max}$; $f_0^{r} = F_{a,\max}$, $f_1^{r} = f_r(t_a^{r} + \Delta t)$, $f_2^{r} = f_r(t_a^{r} + 2\Delta t)$, $\cdots$, $f_{n_r-1}^{r} = f_r(t_a^{r} + (n_r - 1)\Delta t)$, $f_{n_r}^{r} = 0$; $(n_b - 1)\Delta t \le t_{b,n} + t_{\max}^{b}$, $(n_r - 1)\Delta t \le t_{r,n} + t_{\min}^{r}$.

Take air brake application for example, as shown in Figure 2, $n_b = 3$, $f_3^{b} = F_{a,\max}$: if $k = 1$, $F_{a,k}^{b} = u_{b,k} f_0^{b}$; if $k = 2$, $F_{a,k}^{b} = u_{b,k} f_0^{b} + U_{1,k}^{b}(f_1^{b} - f_0^{b})$; if $k = 3$, $F_{a,k}^{b} = u_{b,k} f_0^{b} + U_{1,k}^{b}(f_1^{b} - f_0^{b}) + U_{2,k}^{b}(f_2^{b} - f_1^{b})$; if $4 \le k \le N$, $F_{a,k}^{b} = u_{b,k} f_0^{b} + U_{1,k}^{b}(f_1^{b} - f_0^{b}) + U_{2,k}^{b}(f_2^{b} - f_1^{b}) + U_{3,k}^{b}(f_3^{b} - f_2^{b})$.

Here, $U_{1,k}^{b} = u_{b,k-1} u_{b,k}$, $U_{2,k}^{b} = u_{b,k-2} U_{1,k}^{b}$, $U_{3,k}^{b} = u_{b,k-3} U_{2,k}^{b}$. Also, these logical conditions should be rewritten as the following linear constraints:

$$\begin{cases} U_{1,k}^{b} \le u_{b,k-1}, U_{1,k}^{b} \le u_{b,k}, u_{b,k-1} + u_{b,k} - U_{1,k}^{b} \le 1, \\ U_{2,k}^{b} \le u_{b,k-2}, U_{2,k}^{b} \le U_{1,k}^{b}, u_{b,k-2} + U_{1,k}^{b} - U_{2,k}^{b} \le 1, \\ U_{3,k}^{b} \le u_{b,k-3}, U_{3,k}^{b} \le U_{2,k}^{b}, u_{b,k-3} + U_{2,k}^{b} - U_{3,k}^{b} \le 1, \\ U_{1,k}^{b}, U_{2,k}^{b}, U_{3,k}^{b} \in \{0,1\}. \end{cases} \tag{26}$$

For equation (11), that is,

$$v_{\min,k} \le v_k \le v_{\max,k}, \tag{27}$$

where $v_{\min,k}$ and $v_{\max,k}$ can be calculated based on the minimum release speed v_r and the speed limit $v_{\lim,k}$. Two binary variables $k_{b,k}$ and $k_{r,k}$ are also introduced to indicate the timing of air brake application and release, then ensure that the release time is not less than the air-filled time given in equation (15),

$$k_{b,k} = \begin{cases} 1, \text{if } u_{b,k} - u_{b,k-1} = 1, \\ 0, \text{otherwise.} \end{cases} \tag{28a}$$

$$k_{r,k} = \begin{cases} 1, \text{if } u_{r,k} - u_{r,k-1} = 1, \\ 0, \text{otherwise.} \end{cases} \tag{28b}$$

Thus, logical condition, $[k1 \le k2, k_{b,k2} + k_{r,k1} = 2] \Leftrightarrow [k2 - k1 \ge t_f/\Delta t]$, is expressed as follows:

$$k2 - k1 \ge \left(k_{b,k2} + k_{r,k1} - 2\right) M_2 + \frac{t_f}{\Delta t}, \tag{29}$$

where M_2 is a positive large number, which is introduced to ensure $k2 - k1 \ge t_f/\Delta t$ when $k_{b,k2} = 1$, $k_{r,k1} = 1$, and $k2 \ge k1$ $(1 \le k1 \le N, 1 \le k2 \le N)$. In addition, the binary variable λ_k is introduced to define the neutral section,

$$\lambda_k(s_k) = \begin{cases} 1, s_k \le s_b, \\ 0, s_b \le s_k \le s_e, \\ 1, s_k \ge s_e, \end{cases} \tag{30}$$

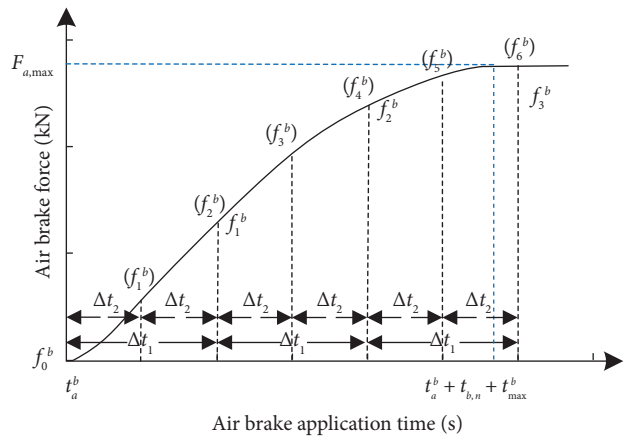

Figure 2: Diagram of air brake force during air brake application.

Then equation (5) can be rewritten as follows:

$$F_{e,k} = \lambda_k u_{e,k} F_{e,\max}. \tag{31}$$

Also, three binary variables are introduced to transform equation (30),

$$\begin{cases} \chi_{1,k} + \chi_{2,k} + \chi_{3,k} = 1, \\ \lambda_k(s_k) = \chi_{1,k} + \chi_{3,k}, \\ s_k \le s_b \chi_{1,k} + s_e \chi_{2,k} + M_3 \chi_{3,k}, \\ s_k \ge s_b \chi_{2,k} + s_e \chi_{3,k}, \\ \chi_{1,k}, \chi_{2,k}, \chi_{3,k} \in \{0,1\}, \end{cases} \tag{32}$$

where M_3 is a positive large number. For equation (31), defining $u_k = \lambda_k u_{e,k}$, and the following linear constraints should be satisfied:

$$\begin{cases} u_k \ge \lambda_k u_{e,\min}, \\ u_k \le \lambda_k u_{e,\max}, \\ u_k \le u_{e,k}, \\ u_k \ge u_{e,k} - u_{e,\max}(1 - \lambda_k), \end{cases} \tag{33}$$

where $u_{e,\min}$ and $u_{e,\max}$ are the minimum and maximum values determined by the control rules.

Finally, the objective function in equation (10) can be rewritten as follows:

$$\min \text{Obj} = w_1 \sum_{k=1}^{N} u_{b,k} \Delta t \frac{1}{T} - w_2 \sum_{k=1}^{N} (s_{k+1} - s_k) \frac{1}{S_{\max}}. \tag{34}$$

The constraints consist of those related to train dynamics (19b), (20), (22a), (22b), and (22c), line slope and curve (23a) and (23b), air brake force (24), (25a), (25b), and (26), and train operation (27), (28a), (28b), and (29)–(33).

Above all, the speed profile optimization problem of the HHT can be transformed into a MILP model. In this paper, the MILP model is solved using CPLEX.

4.3. Balancing the Efficiency and Accuracy. However, the selection of the time interval significantly affects the computation efficiency and accuracy. Smaller intervals enhance solution accuracy at the cost of increased computation time, while larger intervals yield the reverse effect. Specifically, smaller intervals could enable a more detailed consideration of air braking characteristics. As illustrated in Figure 2, assuming $2\Delta t_2 = \Delta t_1$, additional data points from the air brake force curve are employed for modelling. Therefore, this paper proposes a hybrid scheme that combines coarse-grained and fine-grained models to optimize operation strategies. Firstly, the speed profile of HHT running is acquired using a larger time interval, constituting a coarse-grained model. Then, leveraging the calculated solution, a fine-grained model is constructed with a shorter time interval. This sequential refinement leads to improved solutions without significantly prolonging computational time.

Assuming the initial solution with $T = \sum_{k_1=1}^{N_1} \Delta t_1$ is $\{u_{b,1} = 0, \cdots, u_{b,d-1} = 0, u_{b,d} = 1, u_{b,d+1} = 1, \cdots, u_{b,N_1} = 1\}$. Then, we define a search scope, $k_1 \in [d - d', d+d']$, d and d' are positive integers. So when $T = \sum_{k_2=1}^{N_2} \Delta t_2$, it is known that $u_{b,k_2} = 0, k_2 \le (d - d')\Delta t_1 / \Delta t_2$ and $u_{b,k_2} = 1, (d + d')\Delta t_1 / \Delta t_2 \le k_2 \le N_2$. Finally, the solution will be obtained.

5. Case Study

In this section, we employ a 10, 988-tonne HHT with 116 wagons as the subject of our numerical experiments. The partial line information of the actual railway is shown in Figure 3. Other relevant details are given in Tables 4 and 5. The experiments are then carried out on a computer with 3.20 GHz Intel i7 CPU and 16 GB RAM, and CPLEX 12.9.0 is used to solve the proposed model. Also, the computation time is denoted by T_c.

Remark 1. For the sake of simplicity, we define two schemes for the following discussion. Scheme I entails the use of a coarse-grained model or a fine-grained model, while Scheme II involves the combination of coarse-grained and fine-grained models.

Remark 2. Due to the gradual variation in slope gradient and the limited impact of curve resistance, we opt to calculate the line resistance for the entire HHT based on the gradient and curve radius of the foremost position, the first car.

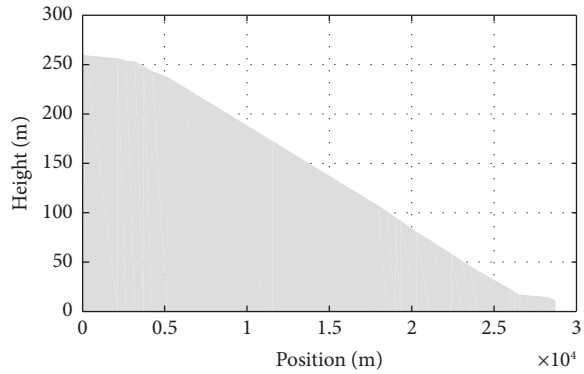

Figure 3: Line information between two stations.

Table 4: Parameters used in numerical experiments.

Parameter	Notation	Value
Given running time (s)	T	1380
Minimum release speed (m/s)	v_r	9.72
Speed limit (m/s)	$v_{\lim}$	20.83
Air-filled time (s)	t_f	180
A positive small number	ε	10^{-9}
Positive large numbers	M_1, M_2, M_3	10^6
A constant about air brake system	C	0.0485
Maximum electric brake force (kN)	$F_{e,\max}$	460

Table 5: Coefficients of the piecewise linear function of basic resistance.

Segment	μ	θ	v (m/s)
1	3.8443	95.2559	9.72–11.25
2	7.6993	51.9998	11.25–20.83

Remark 3. Our primary focus is on scenarios, where the HHT traverses a neutral section with an ongoing air brake application regime, necessitating adherence to the relevant constraint, i.e., $\lambda_k + u_{b,k} \geq 1$.

We then delve into an analysis of the impact of linearization approximation, presenting the average errors between the approximated and true values of both basic resistance and the air brake force in Table 6. Here, we define that error = $|\text{val}_t - \text{val}_a|/\text{val}_t$, where val_a and val_t denote the approximate value and the true value, respectively.

From Table 6, it becomes evident that the linearization methods proposed in this paper yield results that closely approximate the true values. The average approximation errors for basic resistance and air brake force are 1% and 8.9%, respectively. Notably, the 8.9% error is obtained at a time interval of 5 seconds during the air brake application, as an illustration.

5.1. Case 1: Effectiveness Verification. In this case, $w_1 = 0.7$ and $w_2 = 0.3$, and the initial speeds are defined as 13.89 m/s and 19.44 m/s, respectively. Initially, Scheme I is employed to elucidate the impact of the time interval on the HHT operation performance and computation time. In this context, the time intervals are set to 30, 20, 10, and 5 seconds, respectively. Scheme II is then introduced to demonstrate that there is an improvement in efficiency. The experimental results are shown in Tables 7 and 8.

Table 6: Error between the approximated and true values.

Indicator	Basic resistance	Air brake force
Average error	0.01	0.089

Noticeably, in Scheme I, as the time interval decreases, the number of intervals increases, resulting in performance improvements, including increased running distances and reduced air brake application times. This implies that the use of the fine-grained model in conjunction with MILP leads to improved performance. However, this comes at the cost of escalated computation times, surging from 11.29 and 6.55 seconds to over 5000 seconds. Transitioning to Scheme II brings about 91.59% (v_0 is 13.89 m/s) and 91.67% (v_0 is 19.44 m/s) reduction in computation time compared to Scheme I when the time interval is 10 seconds, while preserving performance levels. In particular, when the time interval is 5 seconds, Scheme I struggles to provide solutions within the 5000-second time; with Scheme II, the average time taken is 515.89 seconds. To strike a balanced compromise between operation performance and computation time, a time interval of 5 seconds proves to be optimal for further discussions in Scheme II.

Moving on, Figure 4 shows the relationship between the number of intervals, the objective function, and the computation time for the two initial speeds. Applying Scheme I with a finely tuned time interval results in a marginal improvement in the objective function relative to the substantial increase in computation time. Also, the application of Scheme II improves this situation.

5.2. Case 2: Flexibility Verification. In this case, to clarify the flexibility of Scheme II, we apply it at a time interval of 5 seconds and investigate the performance of different weighting coefficients.

Table 9 presents the optimization results of variable weight coefficients when the initial speeds are set to 13.89 m/s and 19.44 m/s, the number of intervals $N = 276$. Solutions are successfully obtained, averaging around 604.38 and 541.54 seconds for the respective initial speeds. These values markedly exceed those recorded in the scenario with a time interval of 10 seconds. This escalation can be attributed to the significant increase in computational complexity as the number of intervals augments and the search space broadens. Furthermore, for identical initial speeds, as w_2 increases, the air brake application time T_b when $w_1 < w_2$ changes significantly compared to $w_1 > w_2$; as w_1 increases, the running distance is S when $w_1 > w_2$ changes significantly compared to $w_1 < w_2$.

Figure 5 illustrates the speed profiles and corresponding forces as aligned with the results presented in Table 9.

Table 7: Performance comparison of different time intervals with the initial speed 13.89 m/s.

Δt (s)-Scheme	N	Obj	S (m)	T_b (s)	T_c (s)
30-Scheme I	46	0.0779	21705	600	11.29
20-Scheme I	69	0.0454	22875	560	31.72
10-Scheme I	138	0.0400	22901	550	687.72
5-Scheme I	276	—	—	—	5000
10-Scheme II	138	0.0400	22902	550	57.81
5-Scheme II	276	0.0380	23092	550	510.92

Table 8: Performance comparison of different time intervals with the initial speed 19.44 m/s.

Δt (s)-Scheme	N	Obj	S (m)	T_b (s)	T_c (s)
30-Scheme I	46	0.0993	21105	630	6.55
20-Scheme I	69	0.0771	22753	620	18.79
10-Scheme I	138	0.0746	22994	620	705.47
5-Scheme I	276	—	—	—	5000
10-Scheme II	138	0.0745	22996	620	58.75
5-Scheme II	276	0.0717	23028	615	520.86

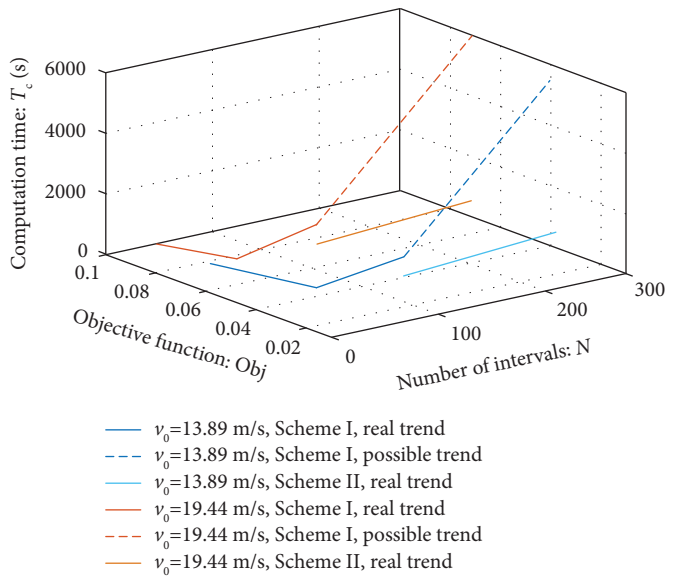

Figure 4: Relationship between the number of intervals, the objective function, and the computation time.

Table 9: Performance comparison of different weight coefficients with the time interval 5 seconds.

v_0 (m/s)	w_1	w_2	Obj	S (m)	T_b (s)
13.89	0.7	0.3	0.0380	23092	550
13.89	1	0	0.3949	22700	545
13.89	0.3	0.7	−0.4421	23202	565
13.89	0	1	−0.8095	23273	590
19.44	0.7	0.3	0.0717	23028	615
19.44	1	0	0.4457	22866	615
19.44	0.3	0.7	−0.4256	23062	625
19.44	0	1	−0.8027	23078	655

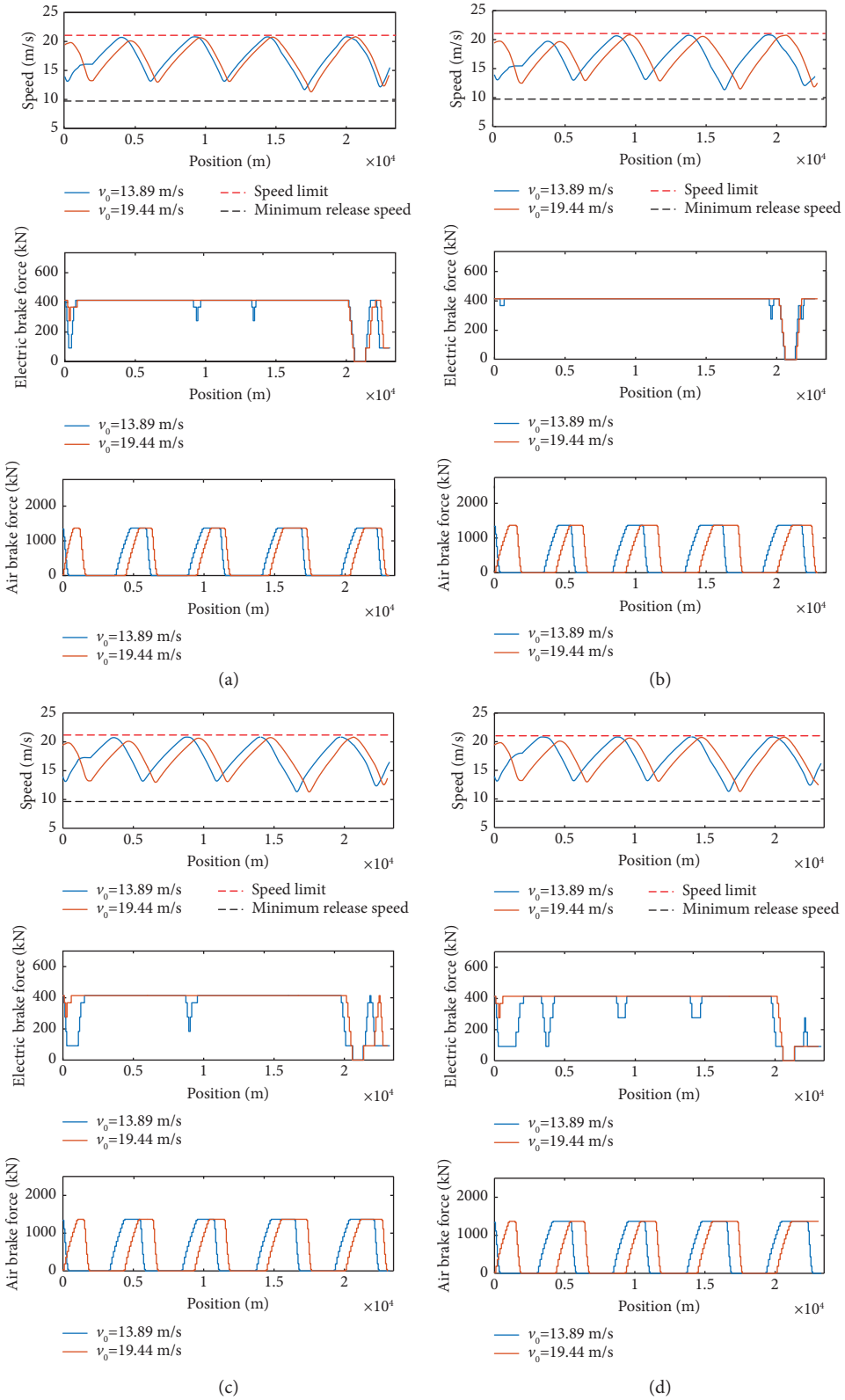

Figure 5: Speed profiles and forces of different initial speeds with different weight coefficients. (a) $w_1 = 0.7$, $w_2 = 0.3$. (b) $w_1 = 1$, $w_2 = 0$. (c) $w_1 = 0.3$, $w_2 = 0.7$. (d) $w_1 = 0$, $w_2 = 1$.

Table 10: Air brake release times of different initial speeds with different weight coefficients. (a) $w_1 = 0.7$, $w_2 = 0.3$. (b) $w_1 = 1$, $w_2 = 0$. (c) $w_1 = 0.3$, $w_2 = 0.7$. (d) $w_1 = 0$, $w_2 = 1$.

Index	v_0 = 13.89m/s				v_0 = 19.44m/s			
	(a)	(b)	(c)	(d)	(a)	(b)	(c)	(d)
1-release time (s)	225	220	195	180	180	180	180	180
2-release time (s)	180	180	180	180	180	185	180	180
3-release time (s)	180	180	180	180	180	180	180	180
4-release time (s)	180	180	180	180	180	180	180	180

In Figure 5, the HHT operates within confines of the speed limit and the minimum release speed. It can be seen that distinct initial regimes manifest with varying initial speeds. However, the influence of the initial speed on the speed profile is progressively mitigated through the coordinated interplay of air braking and electric braking. This trend arises due to the presence of a fixed neutral section around the 20.7 km mark. In accordance with the requirements of operation safety, the HHT control must respect the air brake application regime when traversing the neutral section.

Furthermore, Table 10 provides insights into air brake release times. Notably, a minimum of 180 seconds is allocated for air brake release processes, in compliance with the air-filled time mandate of the train pipe. Noteworthy is the prolonged period required for the initial release of air braking at $v_0 = 13.89$ m/s, serving the purpose of strategic operation adjustment.

On the basis of the above experiments, it is shown that the proposed MILP approach and Scheme II of combining coarse and fine-grained models can address the problem of speed profile optimization well.

6. Conclusions

In this paper, the speed profile optimization problem has been investigated for the safe, efficient, and economical operation of heavy-haul trains (HHTs) on a railway with long and steep downgrades (LSDs). The optimization problem is reformulated as a discrete-time-based mixed integer linear programming (MILP) model, where a set of practical constraints is considered. Specifically, a number of mathematical formulas have been introduced for the air brake application and release process to obtain a more accurate air brake model. Also, for the neutral section, the regime, i.e., air brake application, adapted to the LSDs has been adopted. Moreover, Scheme II, which combines the coarse-grained model and the fine-grained model, has been presented to balance the efficiency and accuracy of the computation. The computational results suggest that the optimal speed profiles of HHTs can be achieved via the mathematical model and solution approach presented.

The proposed method can be used to obtain the speed profile for automatic train operation, which helps to make the operation strategy more realistic, reduce the work intensity of the drivers, and improve the operation speed of HHTs. While the HHT is passing through the neutral section, where the coasting should be followed, we can modify the constraints to ensure the safe and efficient operation.

We focus mainly on the 10, 000-tonne trains with a single locomotive that make up a large proportion in heavy-haul railway. For the application in 20, 000-tonne trains with "1 + 1" formation, which relies on wireless remote multitraction synchronization control, the model in this paper is no longer applicable. In future work, we will extend this research to more complex train formations, such as 30, 000-tonne trains, and we will consider the characteristics of traction, electric braking and air braking, operation rules, and the coupler force that limit train operation. An efficient algorithm will then be developed to solve the optimization model for long train formations.

Data Availability

The data supporting the findings of this study are available from the corresponding author upon reasonable request.

Conflicts of Interest

The authors declare that they have no conflicts of interest.

Acknowledgments

This work was supported by the Fundamental Research Funds for the Central Universities 2023JBZY017 and Scientific and Technological Innovation Program of Shuohuang Railway under Grant nos. 2019-148 and 2021-234, Beijing Laboratory of Urban Rail Transit.

References

[1] A. W. Wardrop, "Autonomous freight trains in Australia," *Proc. 8th Int. Conf. Railway Oper. Model. Anal.-RailNorrköping*, vol. 69, pp. 1120–1130, 2019.

[2] Y. Mazahir, M. Anthony, S. Roslyn, and M. Hiroko, "Heavy haul freight transportation system: autohaul, autonomous heavy haul freight train achieved in Australia," *Technologies to Achieve Smarter Mobility*, vol. 69, no. 6, 2020.

[3] K. Du, Z. Wang, and Z. Zhang, "State observation and parameter identification for autonomous heavy haul train," in *Proceedings of the IEEE Vehicle Power and Propulsion Conference (VPPC)*, pp. 1–5, IEEE, Gijon, Spain, November 2020.

[4] L. Zhang and X. Zhuan, "Optimal operation of heavy-haul trains equipped with electronically controlled pneumatic brake systems using model predictive control methodology," *IEEE Transactions on Control Systems Technology*, vol. 22, no. 1, pp. 13–22, 2014.

[5] J. Yin, T. Tang, L. Yang, J. Xun, Y. Huang, and Z. Gao, "Research and development of automatic train operation for railway transportation systems: a survey," *Transportation*

Research Part C: Emerging Technologies, vol. 85, pp. 548–572, 2017.

[6] B. Jin, S. Yang, Q. Wang, and X. Feng, "Study on energy-saving train trajectory optimization based on coasting control in metro lines," *Journal of Advanced Transportation*, vol. 2023, Article ID 1217352, 12 pages, 2023.

[7] P. Mo, L. Yang, and Z. Gao, "Energy-efficient train operation strategy with speed profiles selection for an urban metro line," *Transportation Research Record*, vol. 2673, no. 4, pp. 348–360, 2019.

[8] Z. Sun and C. Wang, "Security problems of operation heavy haul trains on the long heavy down grade," *Railway Locomotive & Car*, vol. 29, no. 1, pp. 4–7, 2009.

[9] G. Wei, S. Zhu, Y. Wang et al., "Energy efficient automatic train operation for high-speed railways: considering discrete notches and neutral sections," *Transportation Research Part C: Emerging Technologies*, vol. 145, Article ID 103884, 2022.

[10] P. Ying, X. Zeng, A. D'Ariano, D. Pacciarelli, H. Song, and T. Shen, "Energy efficient automatic train operation for high-speed rail-ways: considering discrete notches and neutral sections," *Transportation Research Part C: Emerging Technologies*, vol. 154, Article ID 104202, 2023.

[11] X. Lin, Q. Wang, P. Wang, P. Sun, and X. Feng, "The energy-efficient operation problem of a freight train considering long-distance steep downhill sections," *Energies*, vol. 10, no. 6, p. 794, 2017.

[12] X. Wang, T. Tang, and H. He, "Optimal control of heavy haul train based on approximate dynamic programming," *Advances in Mechanical Engineering*, vol. 9, 2017.

[13] S. Su, W. Liu, Y. Huang, and T. Tang, "Optimization of cyclic air braking strategy for heavy haul trains: an adp approach," in *Proceedings of the 2021 IEEE International Intelligent Transportation Systems Conference IEEE*, pp. 3527–3532, Indianapolis, IN, USA, September 2021.

[14] B. Bai, Z. Xiao, Q. Wang, P. Sun, and X. Feng, "Multi-objective trajectory optimization for freight trains based on quadratic programming," *Transportation Research Record*, vol. 2674, no. 11, pp. 466–477, 2020.

[15] W. Li, S. Jiang, and M. Jin, "Multiobjective optimization and weight selection method for heavy haul trains trajectory," *IEEE Access*, vol. 10, pp. 41152–41163, 2022.

[16] S. Su, Y. Huang, W. Liu, T. Tang, Y. Cao, and H. Liu, "Optimization of the speed curve for heavy-haul trains considering cyclic air braking: an milp approach," *Engineering Optimization*, vol. 55, no. 5, pp. 876–890, 2022.

[17] H. Yu, Y. Huang, and M. Wang, "Research on operating strategy based on particle swarm optimization for heavy haul train on long down-slope," in *Proceedings of the 2018 21st International Conference on Intelligent Transportation Systems (ITSC)*, pp. 2735–2740, IEEE, Maui, HI, USA, November 2018.

[18] H. Yu, Y. Huang, M. Wang, Z. He, X. Meng, and Y. Li, "Research on operating strategies of heavy haul train based on genetic algorithm," *Journal of the China Railway Society*, vol. 42, no. 7, pp. 110–116, 2020.

[19] Y. Huang, S. Su, and W. Liu, "Optimization on the driving curve of heavy haul trains based on artificial bee colony algorithm," in *Proceedings of the 2020 IEEE 23rd International Conference on Intelligent Transportation Systems (ITSC)*, pp. 1–6, IEEE, Rhodes, Greece, September 2020.

[20] Y. Wang, B. Ning, F. Cao, B. De Schutter, and T. J. van den Boom, "A survey on optimal trajectory planning for train operations," in *Proceedings of the 2011 IEEE International Conference On Service Operations, Logistics And Informatics*, pp. 589–594, IEEE, Beijing, China, July 2011.

[21] Y. Wang, S. Zhu, A. D'Ariano, J. Yin, J. Miao, and L. Meng, "Energy-efficient timetabling and rolling stock circulation planning based on automatic train operation levels for metro lines," *Transportation Research Part C: Emerging Technologies*, vol. 129, Article ID 103209, 2021.

[22] B. Benjamin, P. Howlett, P. Pudney, and X. Vu, "Freighmiser: optimal speed profiles for long haul trains," in *Proceedings of the 10th International Conference in Applications of Advanced Technologies in Transportation*, pp. 1–13, Athens, Greece, May 2008.

[23] W. Liu, S. Su, T. Tang, and X. Wang, "A dqn-based intelligent control method for heavy haul trains on long steep downhill section," *Transportation Research Part C: Emerging Technologies*, vol. 129, Article ID 103249, 2021.

[24] Y. Wang, B. De Schutter, T. J. van den Boom, and B. Ning, "Optimal trajectory planning for trains–a pseudospectral method and a mixed integer linear programming approach," *Transportation Research Part C: Emerging Technologies*, vol. 29, pp. 97–114, 2013.

[25] C. Wu, W. Zhang, S. Lu, Z. Tan, F. Xue, and J. Yang, "Train speed trajectory optimization with on-board energy storage device," *IEEE Transactions on Intelligent Transportation Systems*, vol. 20, no. 11, pp. 4092–4102, 2019.

[26] A. D'Ariano, F. Corman, T. Fujiyama, L. Meng, and P. Pellegrini, "Simulation and optimization for railway operations management," *Journal of Advanced Transportation*, vol. 2018, Article ID 4896748, 3 pages, 2018.

[27] M. Feng, C. Wu, S. Lu, and Y. Wang, "Notch-based speed trajectory optimisation for high-speed railway automatic train operation," *Proceedings of the Institution of Mechanical Engineers, Part F: Journal of Rail and Rapid Transit*, vol. 236, no. 2, pp. 159–171, 2022.

[28] Y. Cao, Z. Zhang, F. Cheng, and S. Su, "Trajectory optimization for high-speed trains via a mixed integer linear programming approach," *IEEE Transactions on Intelligent Transportation Systems*, vol. 23, no. 10, pp. 17666–17676, 2022.

[29] Q. Lai, J. Liu, A. Haghani, L. Meng, and Y. Wang, "Energy-efficient speed profile optimization for medium-speed maglev trains," *Transportation Research Part E: Logistics and Transportation Review*, vol. 141, Article ID 102007, 2020.

[30] M. Wei, P. Sun, Q. Wang, Z. Zhang, C. Wang, and C. Zhang, "Adaptive iterative learning for heavy-haul trains trajectory tracking control on long steep downhill sections," in *Proceedings of the 2022 IEEE 17th Conference on Industrial Electronics and Applications (ICIEA)*, pp. 243–249, IEEE, Chengdu, China, December 2022.

[31] Z. Rao, *Train Traction Calculation*, china railway publishing house, Beijing, China, 3rd edition, 2016.

[32] W. J. Davis, *The Tractive Resistance of Electric Locomotives and Cars*, General Electric, Boston, MA, USA, 1926.

[33] W. Liu, S. Su, T. Tang, and Y. Cao, "Study on longitudinal dynamics of heavy haul trains running on long and steep downhills," *Vehicle System Dynamics*, vol. 60, no. 12, pp. 4079–4097, 2022.

[34] H. P. Williams, *Model Building in Mathematical Programming*, John Wiley & Sons, Hoboken, NJ, USA, 2013.